LANGMUIR Article
Cite This: Langmuir 2019, 35, 11114−11122
pubs.acs.org/Langmuir

Direct Assembly and Metal-Ion Binding Properties of Oxytocin Monolayer on Gold Surfaces

Evgeniy Mervinetsky,[†,‡] Israel Alshanski,[†,‡] Jörg Buchwald,[§] Arezoo Dianat,[§] Ivor Lončarić,[∥] Predrag Lazić,[∥] Željko Crljen,*[,∥] Rafael Gutierrez,*[,§] Gianaurelio Cuniberti,[§,⊥,#] Mattan Hurevich,[†,‡] and Shlomo Yitzchaik*[,†,‡]

[†]Institute of Chemistry and [‡]Center for Nanoscience and Nanotechnology, The Hebrew University of Jerusalem, E. Safra Campus, 91904 Jerusalem, Israel

[§]Institute for Materials Science and Max Bergmann Center of Biomaterials, Hallwachsstraße 3, 01062 Dresden, Germany

[∥]Ruđer Bošković Institute, Bijenička cesta 54, 10000 Zagreb, Croatia

[⊥]Dresden Center for Computational Materials Science, TU Dresden, 01062 Dresden, Germany

[#]Center for Advancing Electronics Dresden, TU Dresden, 01062 Dresden, Germany

Supporting Information

ABSTRACT: Peptides are very common recognition entities that are usually attached to surfaces using multistep processes. These processes require modification of the native peptides and of the substrates. Using functional groups in native peptides for their assembly on surfaces without affecting their biological activity can facilitate the preparation of biosensors. Herein, we present a simple single-step formation of native oxytocin monolayer on gold surface. These surfaces were characterized by atomic force spectroscopy, spectroscopic ellipsometry, and X-ray photoelectron spectroscopy. We took advantage of the native disulfide bridge of the oxytocin for anchoring the peptide to the Au surface, while preserving the metal-ion binding properties. Self-assembled oxytocin monolayer was used by electrochemical impedance spectroscopy for metal-ion sensing leading to subnanomolar sensitivities for zinc or copper ions.

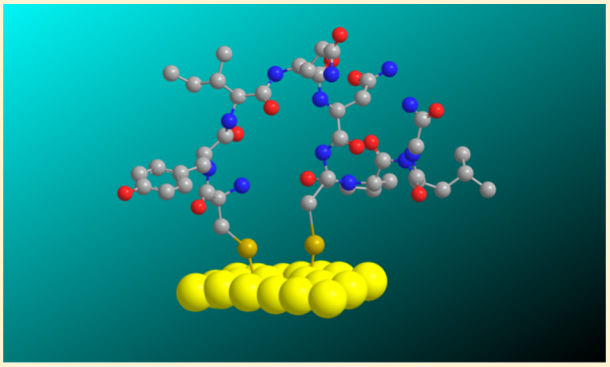

INTRODUCTION

Many peptides are natural binders of metal ions with distinct selectivity and specificity.[1−4] Using peptides as biosensors for metal ions[5−7] or as smart nanomaterials for filtration[8] and purification applications is an emerging and promising approach.[9] These applications require the attachment of the peptides to surfaces.[10,11] Anchoring peptides to surfaces in a way that the inherent metal binding properties are maintained is a synthetic challenge since, in many cases, this process requires chemical modifications of the peptide.[12,13] Developing streamlined processes that will allow for the attachment of native peptides to surfaces without abolishing their metal binding properties is a valuable addition to the field. Using native molecular features in the peptide that are not involved in the biological function, e.g., metal-ion binding, as anchoring moieties to the surface can guarantee that no modification on the peptide has to be made prior to the assembly.

Oxytocin (OT) is an important hormone and neurotransmitter in the human body. OT is a nonapeptide that contains a six-amino-acid cycle and a short tail. The cycle contains a disulfide bond, which is not involved in the metal-ion binding. OT activity is regulated by binding to zinc and copper metal ion and has inherited affinity and selectivity to both ions.[4,14,15] Zinc binding to OT enhances the affinity toward oxytocin receptor (OTR)[15] and hence increases the activity. Copper-ion binding to OT takes place via different binding groups and conformation and leads to reduced affinity toward OTR.[1,16] These ions are important not only for OT binding regulation but also for many biochemical and biophysical processes.[17] Abnormal levels of these two ions can serve as an indicator for immunological and inflammatory disorders, including autism, Alzheimer's disease, multiple sclerosis, skin diseases, and cancer.[18−23] OT-based biosensing for zinc and copper can be a very useful approach in the development of new line of diagnostics. The metal-ion binding properties of OT depend on the peptide's molecular features. It is crucial to preserve these molecular features in the preparation of OT-based sensors.

Recently, we have reported a highly sensitive and selective OT-derived electrochemical biosensor for Cu^{2+} and Zn^{2+} ions.[13,24] The complexation of OT with these metal ions proceeds via different mechanisms: while OT−Cu complex-

Received: June 16, 2019
Revised: July 14, 2019
Published: July 30, 2019

DOI: 10.1021/acs.langmuir.9b01830
Langmuir 2019, 35, 11114−11122

ation involves deprotonation of backbone and square-planar coordination, OT−Zn coordination proceeds with the amides' carbonyl groups and forms a trigonal-bipyramidal complex.[14] In our previous reports, the oxide surface modification with an OT layer was conducted by a multistep assembly process, which resulted in none native triazole-bridged OT. To allow for the attachment to surfaces and the preservation of the metal binding moieties, an additional linker was added synthetically to the OT. We have searched for a simplified route for OT assembly on surfaces. Disulfides and thiols are known to coordinate very strongly to gold surfaces and organized into self-assembled monolayers.[25,26] Chemisorption of the disulfides on Au(111) surfaces results in dissociation of the disulfide bond and formation of two thiolate−gold bonds.[27,28] OT is a peptide that is cyclized by a disulfide bond. We hypothesized that the native disulfide bond of OT can be used for anchoring the peptide to the Au surface without interfering with the metal-ion binding abilities. Herein, we present direct native OT monolayer chemisorption on a gold substrate. We investigate the peptide's assembly and conformational changes upon metal-ion binding applying electrochemistry, spectroscopic ellipsometry, X-ray photoelectron spectroscopy (XPS), Raman spectroscopy, Fourier transform infrared (FTIR) spectroscopy, and contact potential difference (CPD). We analyzed the metal binding potential of the new chemisorbed OT−Au layer to prove that it maintains the native chelation properties. Theoretical modeling was used to characterize the chemisorption and chelation mechanism.

EXPERIMENTAL SECTION

OT Layer Assembly. All solutions used in this work were prepared with Milli-Q Water (18.3 MΩ/cm, Millipore Milli-Q system (Bedford, MA)). The buffer solution used was 50 mM ammonium acetate (pH = 7.0) buffer (AAB) solution (Sigma-Aldrich). Gold surfaces were cast by 70 μL of 250 μM OT (ProSpec-Tany Technogene Ltd., Israel) in AAB for 2 h, then rinsed with AAB and dried under dry N_2 stream. Following peptide assembly, the modified electrodes were exposed to $Cu(NO_3)_2$ (99.999%, trace metal basis, Sigma-Aldrich) and $Zn(NO_3)_2$ (99.999%, trace metal basis, Sigma-Aldrich) AAB solutions in different concentrations.

Surface Characterization. For surface characterization, an Au layer (100 nm) was evaporated on top of Cr layer (10 nm), which evaporated on the substrate of highly doped n-type Si wafer (⟨100⟩, R < 0.003 Ω/cm). The OT layer was adsorbed on this substrate with the same adsorption protocol. Exposure to Cu^{2+}/Zn^{2+} was done by drop casting of metal ions dissolved in AAB. XPS spectra wasrecorded using a monochromatic Al Kα X-ray source on a Kratos Axis-HS instrument. XPS analyses were applied to characterize the self-assembled peptide monolayers and the complexation of the peptide with Cu^{2+}/Zn^{2+} ions. Raman spectroscopy was carried out with a Renishaw inVia Reflex Spectrometer. The Au surface-enhanced Raman spectroscopy (SERS) substrates (SERStrate, Silmeco) were modified with OT layer and have been exposed to Cu^{2+}/Zn^{2+} solution, respectively. Polarization modulation infrared reflection-absorption spectroscopy (PM-IRRAS) measurements were conducted at room temperature under positive nitrogen gas pressure on a reflection-absorption cell (Harrick, Inc.) with a PM-FTIR spectrometer (PMA-50 coupled to Vertex V70, Bruker). The signal was collected from modified Au surfaces by 2048 scans with a resolution of 4 cm^{-1} using a mercury cadmium telluride detector. CPD measurements were performed with Kelvin probe S (DeltaPhi Besocke, Jülich, Germany), with a vibrating gold electrode (work function (WF), 5.1 eV) in a home-built Faraday cage under argon atmosphere. Variable angle spectroscopic ellipsometry measurements were carried out with ellipsometer VB-400 (Woollam Co.) at the Brewster angle of 75°. AFM (Bruker, Innova) was performed in tapping mode to monitor topography homogeneity of the layer as a result of OT adsorption and metal-ion chelation.

Electrochemical Characterization. Electrochemical analyses were conducted with Bio-Logic SP-300 potentiostat (Bio-Logic Science Instruments, France), utilizing electrochemical impedance spectroscopy (EIS) and cyclic voltammetry (CV) with EC-LAB software package. A three-electrode cell was used for the measurements: Ag/AgCl (in 3 M KCl) as reference electrode, Pt as counter electrode, and Au as working electrode (WE). Polycrystalline bulk gold electrodes with 2 mm diameter were used for electrochemical measurements (CH Instruments). These electrodes were manually polished on micro-cloth pads (Buehler, Lake Bluff, IL) with deagglomerated alumina suspension (Buehler) of decreasing particle size (1.0 and 0.05 μm) and washed with TDW. Then, Au WE was cast by OT by the described protocol. EIS measurements were performed at three stages: bare gold electrode, after adsorption of the peptide to the gold electrode, and finally after exposure to metal ions. The frequency range is 100 kHz to 0.1 Hz with E_{we} = 0.21 V according to Ag/AgCl reference electrode. All EIS scans were done in EIS solution of 5.0 mM $K_3[Fe(CN)_6]$, 5.0 mM $K_4[Fe(CN)_6]$ (RedOx species), and 0.1 M KCl as supporting electrolyte in 50 mM AAB solution. The results fitted with the circuit $R_S[(R_{CT}|W)||Q]$, where Q is a constant phase element, which describes a nonideal capacitor. For dose response, exposure of the Au−OT electrode was followed by its dipping in ion solution in AAB for 10 min, washing with the buffer (by rinsing the electrode with 1 mL of AAB by Pasteur pipette), EIS measurement, and further exposure for increasing concentrations of ions in AAB. The data were presented based on statistics of three different electrodes. CV analysis was done on Au−OT electrode and Au−OT electrode after exposure to 10 μM Cu^{2+}/AAB solution. The electrolyte solution was 0.1 M KCl in 50 mM AAB solution. The scan was done between −0.8 and +0.8 V with various scan rates: 10, 50, 100, and 150 mV/s. Reductive desorption analysis[26,29,30] was performed for determination of surface coverage of OT on Au electrode. This characterization was done by CV in KOH [0.5 M] electrolyte with degassing by N_2 for 5 min prior to the analysis. The CV was recorded between −0.5 and −1.4 V with a scan rate of 100 mV/s.

Computational Methods. *Classical Molecular Dynamics (MD).* MD simulations were carried out using the force field developed by the Heinz group to describe the Au(111) surface.[31] Therein, the interaction between Au atoms is described by a Lennard-Jones potential. The force-field parameters for oxytocin were computed using the Automated Topology Builder (ATB) to generate the necessary GROMOS force-field parameters.[32] For this purpose, we use fragmentation and the transferability of the GROMOS force field to obtain atomic charges from a Merz−Singh−Kollman (MK) scheme on the B3LYP/6-31G* level of density functional theory (DFT) theory.[33] The fragmentation was done such that every fragment was smaller than 50 atoms and all fragments overlap each other. All MD simulations were performed using the GROMACS software. A periodic supercell with a size of 74 nm^3 was first equilibrated for 300 ps, followed by Nosé−Hoover thermostating at 300 K within an NVT ensemble.[34,35]

Density Functional Theory Calculations. For DFT calculations, a mixed Gaussian plane-wave method was used, as implemented in the CP2K software.[36−38] For all DFT calculations, a mixed basis set approach is used, where the Kohn−Sham orbitals are expanded into linear combinations of contracted Gaussian-type orbitals and complemented by a plane-wave basis set to compute the electronic charge density. The norm-conserving pseudopotential GTH (Goedecker, Teter, and Hutter) was used.[39,40] In the case of Zn^{2+} binding to oxytocin, benchmarking showed that the LDA-PADE exchange−correlation functional was more appropriate for structural relaxation. For the work function calculations, however, the Perdew−Burke−Ernzerhof (PBE) functional was used. A DZVP (double zeta for valence electrons plus polarization functions) basis set complemented with a plane-wave basis set energy cutoff 350 Ry was further adopted. Nudge elastic band (NEB) calculations with climbing image method were performed with the ATK-DFT code using the PBE exchange−

DOI: 10.1021/acs.langmuir.9b01830
Langmuir 2019, 35, 11114−11122

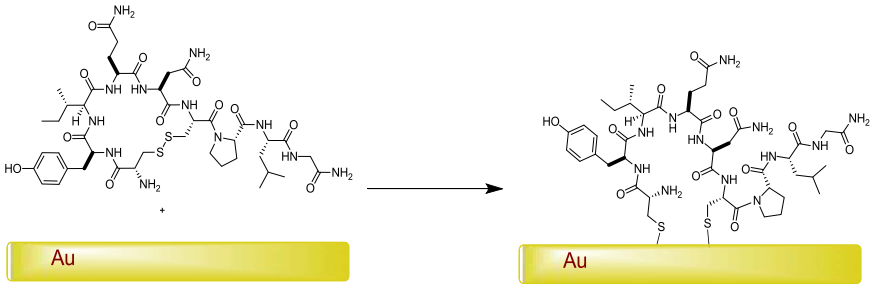

Figure 1. Chemisorption of OT via disulfide oxidative addition to Au surface forming Au−OT.

correlation functional with Grimme D2 dispersion corrections and SG15 pseudopotentials.[41−45]

RESULTS AND DISCUSSION

Direct chemisorption of the native neuropeptide OT was used on gold surface through disulfide bridge dissociation followed by S−Au bond formation (Figure 1). We have used various analytical methods to characterize the assembled monolayer and to evaluate the metal binding properties of the chemisorbed OT.

Surface Analysis. Anchoring of the OT to the gold surface through disulfide dissociation and S−Au bond forming was investigated first by surface-enhanced Raman spectroscopy (SERS). SERS analysis was conducted on the Au−OT surface to characterize and identify the OT surface anchoring and ion binding (Figure 2). A peak at 285 cm^{-1} was assigned to S−Au

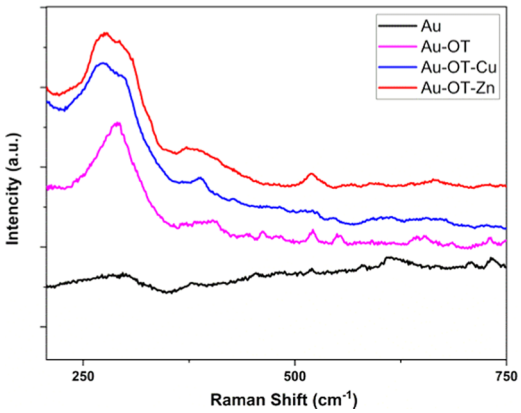

Figure 2. Surface-enhanced Raman spectroscopy of bare Au (black), Au−OT (magenta), Au−OT after exposure to Cu^{2+} solution [10 μM in AAB] (blue), and Au−OT after exposure to Zn^{2+} solution [10 μM in AAB] (red).

bond.[46,47] This peak is significantly higher for Au−OT surfaces compared to bare Au SERS surface washed with AAB (Figure 2, black curve). The presence of the characteristic gold−sulfur bond energy by SERS and the absence of the disulfide bond-related energy[48] at 420−520 cm^{-1} (observed by attenuated total reflection (ATR)-FTIR of OT; see Figure S1) confirm chemisorption to gold by oxidative addition.

SERS was also used to characterize peptide-ion interactions (Figures 2 and S2). An absorption in the 270−280 cm^{-1} spectral region was observed after exposure of the OT layer to copper or zinc ions. This new absorption is indicative of changes in sulfur−metal vibrations.[49,50] A new absorption was observed at 389 cm^{-1} after exposure to copper. Since absorption at 350−400 cm^{-1} spectral region is usually indicative of a deprotonated amide−Cu bonding,[51,52] the Raman peak at 389 cm^{-1} (Figure 2, blue curve) can be related to $N^{-}-Cu^{2+}$ bonding.

XPS analysis of samples with chemisorbed OT presents a significant peak at binding energies of 400 and 163.5 eV. These peaks related to N 1s (Figure S3) and S 2p (Figure S4), respectively. These signals are absent in the scan of bare Au substrate. This presence of N and S peaks on the surface can only be attributed to the adsorption of OT to the Au substrate. Moreover, analysis of bare Au represents only C 1s-related peak at 284.2 eV (Figure S5). This peak may be attributed to some carbon impurities. However, analysis of Au−OT surfaces (Figure S6) clearly represents convolution of C 1s peaks at 284.8, 286.06, and 288.13 eV. These peaks are indicated as C−C, C−N/C−O, and O=C−N respectively[53] and hence serve as an evidence for the presence of peptide on the surface.

Ellipsometry analysis shows an organic layer thickness of 1.42 nm with good fit (MSE = 3.8) for the OT layer on gold substrate. Ellipsometric analysis is in agreement with XPS thickness measurement of 1.41 nm for OT monolayer. These thickness analyses are compatible with the calculated cross section of OT of ∼1 nm, suggesting a stronger vdW-mediated molecule−surface interaction compared to the experiments. Thickness measurements support OT monolayer formation with the longitudinal axis of the peptide parallel to the surface. To measure surface roughness and to verify the homogeneity of the surface, AFM analysis was performed for all modification steps (Figure S9). AFM shows that in all of the assembly steps, the surface topography is smooth and without defects or pin holes. One can see surface smoothening following OT assembly[54,55] and roughening following copper-ion binding.[5] The AFM analysis adds to the ellipsometry and XPS results proving the formation of OT monolayer.

XPS was used to characterize the peptide layer upon the chelation with Cu^{2+}/Zn^{2+} ions (see Figures S7 and S8). A peak at 1022.2 eV was observed only for the OT layer after exposure to Zn^{2+} ions. This peak is related to Zn^{2+} $2p_{3/2}$ and is shifted by about −0.5 eV relative to the free ion[56] (Figure S7). A peak at 932 eV was observed after exposure of OT−Au to copper ions (Figure S8). Such energy corresponds to the Cu^{2+} $2p_{3/2}$ binding energy and is slightly shifted from the typical XPS Cu^{2+} peak (933.6 eV). This peak can be attributed to the chelation with the OT peptide by copper; hence, it is an indication that the peptide on the surface chelates the ion.[57] XPS analysis of the nitrogen atom represents a single peak at 400.1 eV (Figure S3), which can be attributed to nitrogen in amide or amine bonds.[58] There is no spectral evidence for nitrogen at binding energy of about 407 eV characteristic for nitrogen in nitrate (N−O) residues.

DOI: 10.1021/acs.langmuir.9b01830
Langmuir 2019, 35, 11114−11122

Cyclic Voltammetry Analysis of OT Layer with Cu^{2+}. To confirm OT−Cu^{2+} chelation, a direct measurement of metal ions on the surface was performed by cyclic voltammetry (CV; see Figure 3).

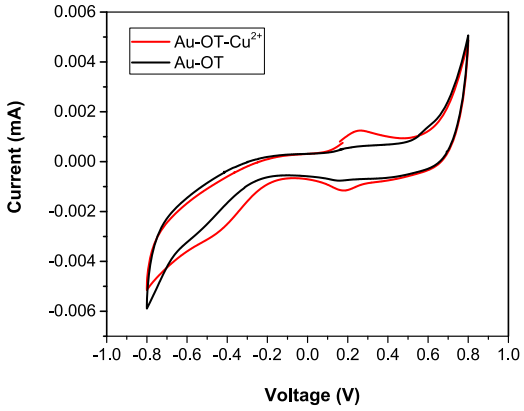

Figure 3. CV of Au−OT electrode (black) and Au−OT−Cu^{2+} electrode (red) prepared by exposure to 10 μM Cu^{2+} solution. The CV was performed in KCl [0.1 M] in AAB [50 mM, pH = 7] with scan rate of 100 mV/s.

By this analysis, we directly recognize an indicative Cu^{2+} oxidation peak at 0.26 V, which is significantly shifted from the oxidation peak of free Cu^{2+} ion (0.12 V). We can attribute the shift to OT−Cu complex formation.[59] Moreover, CV with various scan rates (Figure S17) represents linear dependence of current on scan rate (Figure S18), which is characteristic for surface-bound redox centers. From the CV data, we were able to calculate the number of ions and surface concentration of the cooper ions in the layer according to eq 1

$$M^{z+} = \frac{Q \times C}{A \times z} \quad (1)$$

where M^{z+} is the amount of metal ions, z is the valence of the metal ions, Q is the charge transfer (calculated by the integral of the CV peak), C is the Coulomb constant, and A is the area of the electrode. By calculating the amount of copper on the surface, we obtain a copper-ion surface concentration of 0.75 ions/nm^2 in the monolayer.

Reductive desorption[26,29,30] was done to measure the number of OT molecules. The characteristic peak at −1.1 V (Figure S15) indicates the reduction of S−thiol bond from Au surface. Since each OT molecule has two S−Au bonds, reduction of each molecule attributes with two electrons. The calculated footprint of OT is 2.76 nm^2 (see the SI) when the modeling of OT described 2.5 nm^2.

CV analysis yielded a Cu^{2+}-to-OT ratio of 2:1. The CV analysis confirmed the presence of OT on the gold surface and the complexation between copper and the peptide.

PM-IRRAS Analysis of OT Monolayer. Polarization modulation IR reflection-absorption spectroscopy measurements were performed to identify the changes in orientation of the specific functional groups.

The intensity difference of the peaks represents dissimilar polarization of the band, namely, the subtraction of s-polarized beam, which is parallel to the surface of the sample from p-polarized beam, which is perpendicular to the sample surface.[60] Hence, the alterations in PM-IRRAS spectra can be attributed to different molecular orientations,[61] associated with the conformational changes in peptide layer. We used the PM-IRRAS to monitor conformational changes of the OT monolayer after ion binding (see Figure 4).

We focused mostly on changes of signals in two regions, namely, amide I and amide II. The amide I band (1600−1700 cm^{-1}) is attributed to the C═O stretching vibration of the amide groups and to in-plane N−H bending. The amide II band (1480−1575 cm^{-1}) derives mainly from in-plane N−H bending and from the C−N stretching vibration. The amide I spectral region is sensitive to the changes in peptide conformations, while the amide II band is less sensitive to these changes.[62]

Differences in OT spectra as a function of exposure to metal ions are observed in the amide I (1620−1750 cm^{-1}) and amide II (1530−1600 cm^{-1}) regions. A significant increase in absorbance at 1745 cm^{-1} in the OT spectra was observed after exposure to Cu^{2+} and Zn^{2+}. These indicate that significant conformational changes take place at the amide groups of the peptide monolayer. Interestingly, only after exposure of the monolayer to Zn^{2+}, a sharp decrease in absorbance of the amide I region (at 1684−1726 cm^{-1}) was observed (Figures 4B and S10). Since this band is related to the orientation of the carbonyl groups, the observed change in orientation supports our hypothesis that OT binds zinc ions via carbonyl groups, in agreement with the suggested binding mechanism and peptide conformational changes.

Additional changes were detected in 1480−1430 cm^{-1} (C−N groups[63]) and 1300−1500 cm^{-1} (amide fingerprint[63])

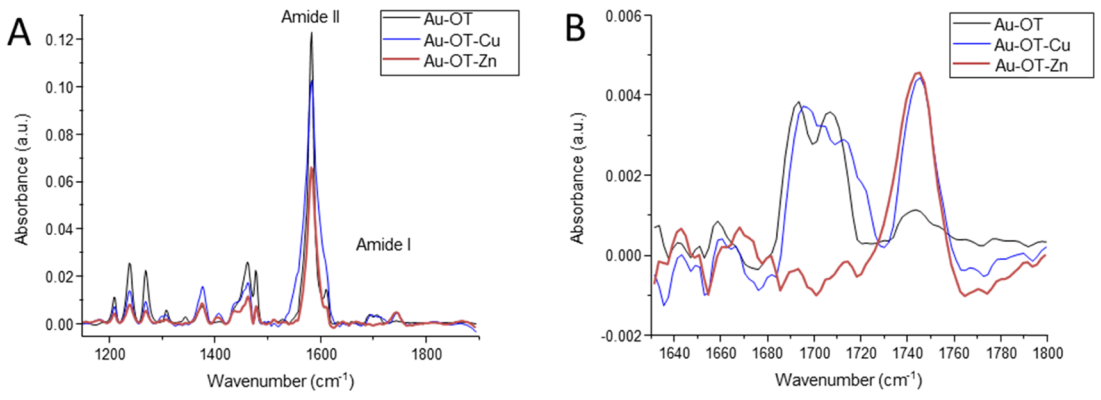

Figure 4. PM-IRRAS: entire scan (A) and amide I region (B) of OT layer (black); OT after exposure to Cu^{2+} solution [10 μM in AAB] (blue); and OT after exposure to Zn^{2+} solution [10 μM in AAB] (red).

DOI: 10.1021/acs.langmuir.9b01830
Langmuir 2019, 35, 11114−11122

regions, which further supports our assumption that this ion binding induces conformational changes (see also ATR spectra; Figure S1).

Computational Modeling. To explore the representative conformational space of native OT as well as oxytocin on flat Au(111), we performed MD simulations at T = 300 K. Moreover, we have also considered the influence of Cu^{2+} and Zn^{2+} binding to the OT conformation, both in the native state and on Au(111). The ability of free and surface-adsorbed OT to bind Cu^{2+} and Zn^{2+} ions via deprotonated amides and via carbonyls, respectively, supports our experimental findings and is in good agreement with other studies.[14] The results of the classical MD simulations are summarized in the Supporting Information (Figures S11 and S12). In what follows, we exclusively focus on DFT-based calculations of the ion binding energetics.

Chemisorption of Oxytocin on Au(111). State-of-the-art knowledge of gold−sulfur interfaces identified a bridging Au atom between sulfur atoms as a key structural unit.[64] Therefore, we also modeled oxytocin on Au(111) with one adatom as a minimal model of a more realistic surface. As shown in Figure 5, NEB calculations of the minimum energy path show that there is no significant barrier for dissociation of the disulfide bond and chemisorption of oxytocin over Au(111) with an adatom takes place (see also Movie S1). There is an energy gain of more than 4 eV per molecule upon chemisorption, and the Au adatom makes a bridge between the two S atoms[64] with a S−Au bond of 2.3 Å and a S−Au−S bonding angle of 136°. The absence of the dissociation barrier is a good explanation of the clear presence of the S−Au peak in Raman analysis presented in the Experimental Section.

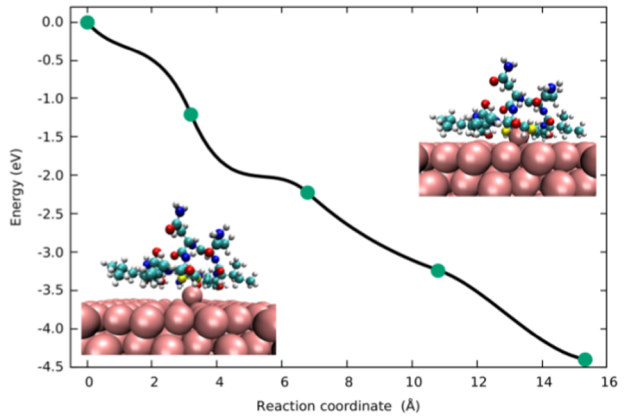

Figure 5. Nudge elastic band calculation of the minimum energy path shows no barrier for disulfide bond dissociation on Au(111) with an adatom. The bottom left inset shows the initial nondissociated structure, while the top right inset shows the final structure with the broken disulfide bond.

Binding of Cu^{2+} to Oxytocin. The binding cascade initiated by Cu^{2+} is addressed here, first for native OT. Cu^{2+} initially binds to the neutral N-terminal amino and then to three additionally deprotonated amides before reaching the most stable square planar conformation. For the first reaction step in which Cu^{2+} binds to the amino group, we considered a small water cluster (three water molecules) near the Cu^{2+}. Upon deprotonation of the amide groups and the formation of Cu−N bonds, the water molecules were subsequently removed from the simulation box.

The ion binding energy is computed as the total energy difference between the chelated system and the system in which ion + water is placed in the cell at a distance of about 20 Å from the OT molecule. The cascade reaction of Cu^{2+} is shown in Figure 6 for 1- to 4-fold coordination. We then addressed the binding of Cu^{2+} to OT attached to the gold surface. A summary of our results for free (native) OT and OT on the Au(111) surface is shown in Figure 7. The binding energy increases with increasing number of bonds between Cu^{2+} and the deprotonated amide groups for both cases, free OT and OT on the surface, although we found a slightly larger ion binding strength to OT on the surface. This can be attributed to the reduction of the conformational freedom due to the chemisorption process on the surface.

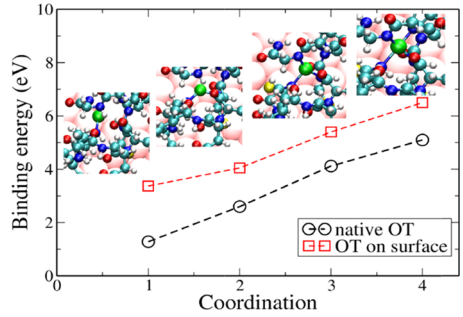

Figure 7. Binding energies associated with the binding cascade of Cu^{2+} ions to free OT and to OT on the Au(111) surface.

Binding of Zn^{2+} to Oxytocin. We have carried out a similar analysis for Zn^{2+} binding (see Figure 8). We find that the ion binding coordination remained trigonal-bipyramidal, involving four carbonyls and the N-terminal amino. A binding energy of 0.09 eV was initially calculated using the PBE XC functional. As this value seems to be unphysically low, we attribute the effect to be an artifact of the used GTH pseudopotential. Hence, we performed additional calculations using the LDA-PADE XC functional taking only two valence electrons into account.[39] Here, we obtained a rather high value of 8.47 eV. For the purpose of cross-checking, we further computed the corresponding binding energy for the Cu^{2+} chelation to OT using this functional and obtained a value

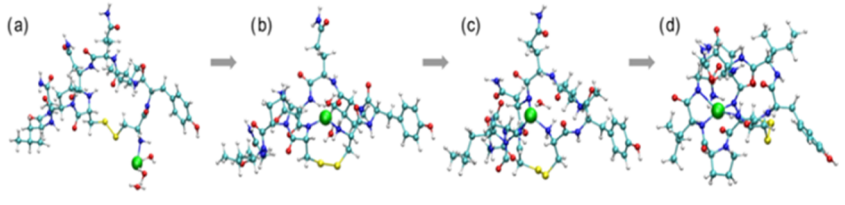

Figure 6. Binding cascade of Cu^{2+} to native oxytocin.

DOI: 10.1021/acs.langmuir.9b01830
Langmuir 2019, 35, 11114−11122

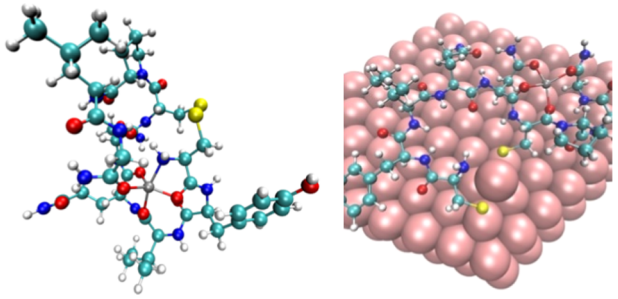

Figure 8. Left: free oxytocin chelated in a trigonal-bipyramidal structure to a Zn^{2+} ion via four carbonyls and the terminal amino. Right: oxytocin on Au(111) with Zn^{2+} chelated in a trigonal-bipyramid conformation.

of 6.75 eV, which is also higher than the value found with the PBE functional. These results are most likely related to an overestimation of the LDA exchange−correlation effects, while the structural information nearly remains.

For the surface-attached OT, strong conformational changes seem to be restricted due to the interaction of the molecule with the surface. As a result, MD simulations showed that Zn^{2+} was less coordinated compared to the native OT case. After a DFT-based energy minimization, we found that Zn^{2+} dissolved from the terminal nitrogen and chelated with two other carbonyl oxygen atoms nearby. From the binding angles of about 100°, we concluded that Zn^{2+} chelates in a quasi-tetrahedral structure. A rather weak binding energy was obtained (binding energy of 1.68 eV), in clear contrast to the Cu^{2+} case (binding energy of 5.08 eV; see also Figure 8 and Table S1). We attribute this result to the more peripheral position of the Zn^{2+} ion as well as to the less stable tetrahedral chelation achieved on the surface (compared to the trigonal-bipyramidal chelation found for free OT with Zn^{2+} in water).

Work Function Changes upon Ion Binding. The work function (WF) change of the surface is directly proportional to the change in the surface electric dipole caused by the adsorption of molecules.[65−67] Thereby, a strong correlation exists between the molecular dipole moments and the WF change induced by adsorbed molecules on metal and semiconductor surfaces.[68−70] The WF is defined as the difference between electrostatic potentials at the vacuum level and at the Fermi energy of the surface. In Figures S13 and S14, the corresponding WFs as a function of the z coordinate (perpendicular to the surface) are presented. The calculated WF of pure Au(111) of 5.28 eV is in very good agreement with other theoretical and experimental works.[71] The presence of OT on the surface leads to a WF change depending on its conformation. As we found quite different conformations in the MD simulation for the neutral OT and the deprotonated OT, we see that this transfers to the work functions as well. Therefore, we need to take these different WFs as reference points. In this case, we find a decrease of the WF, which is of the same order of magnitude (see Table 1). While Cu^{2+} binding leads to an increase of the WF by 0.76 eV, Zn^{2+} binding induces a WF reduction by 0.93 eV.

The WF changes were experimentally determined by Kelvin Probe CPD. It was found that after OT−Cu^{2+} chelation, the WF increased by 49 meV, while OT−Zn^{2+} complexation resulted in a decrease of the WF by 54 meV (Figure 9).

These experimental observations are explained by the different chelation mechanisms of OT with Cu^{2+} and Zn^{2+}.

Table 1. Calculated Work Function Change upon Ion Binding[a]

Au−OT	Au−OT−Zn^{2+}	Au−OT−Cu^{2+}
−0.48 eV	−1.41 eV	+0.28 eV

[a]The indicated values are relative to Au(111) surface.

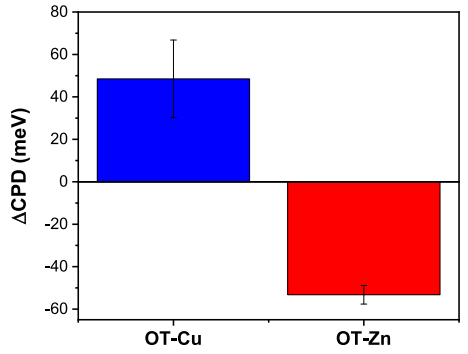

Figure 9. CPD measurements of Au−OT surface after exposure to copper ions (blue) and Au−OT after exposure to Zn^{2+} ions (red).

The formation of OT−Cu complex involves deprotonation of amide bonds that causes a net negative charge (−1) of the complex. This results in an increase of the WF. However, the complex formation of OT−Zn does not go through deprotonation. Hence, the positive charge of the complex (+2) causes a decrease in WF. The theoretical calculations and experimental measurements displayed similar qualitative trends, with albeit some differences in the values. Our lower experimental values might be due to strong depolarization effects[67] that are the result of intermolecular interaction in a monolayer diluting the net dipole and thus the change of the work function.[72,73]

Dose Response of OT to Copper and Zinc Ions Measured by EIS. To evaluate the interaction of OT monolayer with copper and zinc ions, OT−Au electrodes were introduced to various concentrations of the metal ions and the EIS response was measured (Figures S19 and S20). The measured R_{CT} values were normalized to initial R_{CT} value of the electrode before exposure to metal ions. Exposure time to the metal-ion solution was relatively long (10 min) to nullify the influence of kinetics.

From these results, a plot of normalized R_{CT} values as a function of the ion concentration was made to represent the dose response of the sensing device (Figure 10).

The OT sensor showed sensitivity to both metal ions in a wide range of concentrations. For Cu^{2+}, the dynamic range observed for concentrations of 10^{-13}−10^{-9} M. For Zn^{2+} ions, the sensitivity was detected from 10^{-13} to 10^{-3} M. The increase of R_{CT} values resulted from conformational changes of peptide layer upon metal-ion binding. The saturation region of OT−Cu response from nM to mM region is achieved at 1:2 ratio between OT and copper ions, as suggested by CV analysis, while OT−Zn coordination through carbonyl groups did not exhibit saturation suggesting complexation that approaches 1:1 ratio. The label-free metal-ion sensing described above proved that using native OT attached to gold substrate can be useful for biosensing applications.

DOI: 10.1021/acs.langmuir.9b01830
Langmuir 2019, 35, 11114−11122

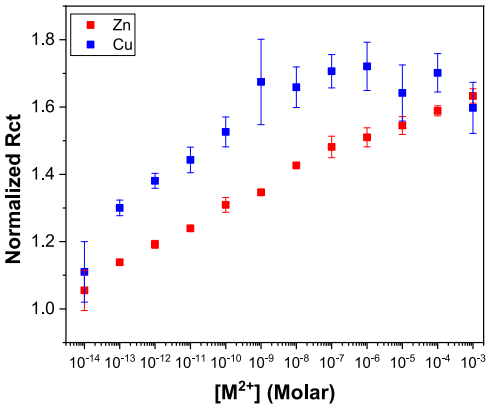

Figure 10. EIS-derived dose response of OT sensor to Cu^{2+} ions (blue curve) and Zn^{2+} ions (red curve). R_{CT} values after exposure to metal-ion solutions normalized by the initial R_{CT}. The frequency range is 100 kHz to 0.1 Hz with E_{we} = 0.21 V according Ag/AgCl reference electrode. All EIS scans were done in EIS solution of 5.0 mM $K_3[Fe(CN)_6]$, 5.0 mM $K_4[Fe(CN)_6]$ (RedOx species), and 0.1 M KCl as supporting electrolyte in 50 mM AAB solution.

CONCLUSIONS

In this study, we presented a new strategy for the assembly of native neuropeptide on gold surfaces. We developed a simple method for single-step fabrication of OT monolayers on gold substrates. We used an unmodified native peptide and utilized the disulfide group for direct anchoring to the surface and its other functional groups for metal-ion binding. The conformational changes of the peptide layer resulting from chelation of OT with metal ions were confirmed and characterized by electrochemical, spectral, and theoretical calculations. In this work, we showed that direct adsorption of native OT via disulfide bond to step-edge regions of the gold surface allowed for the preservation of the peptide functionality. Furthermore, the absence of a dissociation barrier of the disulfide bond of OT on the gold surface with an adatom supports the experimental claim that OT is chemisorbed on Au via Au−S bonds. Our study suggests that the assembly strategy preserves native metal-ion chelation properties. This indicates that native neuropeptides immobilized on the surface can be a very useful biomimetic tool.[74] Our strategy could be applied for studying biorelevant interactions of this extremely important neuropeptide. The use of atomistic methodologies complementing the experimental studies has helped to shed light on the various possible coordination environments of Cu^{2+} and Zn^{2+} upon binding to OT on the Au substrate as well as to highlight the differences to the native (i.e., free) OT. The computed binding energies of Cu^{2+} and Zn^{2+} to OT on Au(111) suggest a stronger binding of Cu^{2+} to OT. This work shows that using native functional groups of peptides for direct assembly on gold can be highly useful for novel bioelectronic architectures and neuromorphic computing. The envisioned application of this model system can be extended for interaction of OT with OT-receptor probing and studying other binding proteins in the presence and absence of different metal ions. In addition to flat surfaces, this model can be used on nanoparticles for bioimaging applications.

ASSOCIATED CONTENT

Supporting Information

The Supporting Information is available free of charge on the ACS Publications website at DOI: 10.1021/acs.langmuir.9b01830.

NEB calculations of the minimum energy path show that there is no significant barrier for dissociation of the disulfide bond and chemisorption of oxytocin over Au(111) with an adatom takes place (AVI)

AFM, SERS, ATR-FTIR, DFT calculations, additional electrochemical data, XPS analysis (PDF)

AUTHOR INFORMATION

Corresponding Authors

*E-mail: Zeljko.Crljen@irb.hr (Z.C.).
*E-mail: rafael.gutierrez@tu-dresden.de (R.G.).
*E-mail: shlomo.yitzchaik@mail.huji.ac.il (S.Y.).

ORCID

Evgeniy Mervinetsky: 0000-0002-4373-1263
Israel Alshanski: 0000-0002-9310-1921
Ivor Lončarić: 0000-0002-5554-4641
Rafael Gutierrez: 0000-0001-8121-8041
Gianaurelio Cuniberti: 0000-0002-6574-7848
Mattan Hurevich: 0000-0002-1038-8104
Shlomo Yitzchaik: 0000-0001-5021-5139

Author Contributions

The manuscript was written through contributions of all authors. All authors have given approval to the final version of the manuscript.

Funding

This investigation was carried out with financial support of the H2020-FETOPEN project Reservoir Computing with Real-time Data for future IT (RECORD-IT) under grant no. 664786. I.L., P.L., and Ž.C. were also supported by the European Union through the European Regional Development Fund—the Competitiveness and Cohesion Operational Programme (KK.01.1.1.06) and the H2020 CSA Twinning project No. 692194, RBI-T-WINNING.

Notes

The authors declare no competing financial interest.

ACKNOWLEDGMENTS

S.Y. is the Binjamin H. Birstein Chair in Chemistry. This research was partly supported by the German Research Foundation (DFG) within the Cluster of Excellence "Center for Advancing Electronics Dresden". TU Dresden gratefully acknowledges computing time by the Center for Information Services and High Performance Computing (ZIH). The authors thank Dr. Vitaly Gutkin for XPS analysis, and Shahar Dery and Dr. Elad Gross for FTIR analysis.

REFERENCES

(1) Kozłowski, H.; Bal, W.; Dyba, M.; Kowalik-Jankowska, T. Specific Structure−Stability Relations in Metallopeptides. *Coord. Chem. Rev.* **1999**, *184*, 319−346.
(2) Pavan, S.; Berti, F. Short Peptides as Biosensor Transducers. *Anal. Bioanal. Chem.* **2012**, *402*, 3055−3070.
(3) Xiang, D.; Wang, X.; Jia, C.; Lee, T.; Guo, X. Molecular-Scale Electronics: From Concept to Function. *Chem. Rev.* **2016**, *116*, 4318−4440.

DOI: 10.1021/acs.langmuir.9b01830
Langmuir 2019, 35, 11114−11122

(4) Sigel, H.; Martin, B. Coordinating Properties of the Amide Bond. Stability and Structure of Metal Ion Complexes of Peptides and Related Ligands. *Chem. Rev.* **1982**, *82*, 385−426.
(5) Mervinetsky, E.; Alshanski, I.; Hamo, Y.; Sandonas, L. M.; Dianat, A.; Buchwald, J.; Gutierrez, R.; Cuniberti, G.; Hurevich, M.; Yitzchaik, S. Copper Induced Conformational Changes of Tripeptide Monolayer Based Impedimetric Biosensor. *Sci. Rep.* **2017**, *7*, No. 9498.
(6) Gooding, J. J.; Hibbert, D. B.; Yang, W. Electrochemical Metal Ion Sensors. Exploiting Amino Acids and Peptides as Recognition Elements. *Sensors* **2001**, *1*, 75−90.
(7) Mervinetsky, E.; Alshanski, I.; Lenfant, S.; Guerin, D.; Medrano Sandonas, L.; Dianat, A.; Gutierrez, R.; Cuniberti, G.; Hurevich, M.; Yitzchaik, S.; Vuillaume, D. Electron Transport through Self-Assembled Monolayers of Tripeptides. *J. Phys. Chem. C* **2019**, *123*, 9600−9608.
(8) Papp, S.; Jágerszki, G.; Gyurcsányi, R. E. Ion-Selective Electrodes Based on Hydrophilic Ionophore-Modified Nanopores. *Angew. Chem.* **2018**, *130*, 4842−4845.
(9) Yitzchaik, S.; Gutierrez, R.; Cuniberti, G.; Yerushalmi, R. Diversification of Device Platforms by Molecular Layers: Hybrid Sensing Platforms, Monolayer Doping, and Modeling. *Langmuir* **2018**, *34*, 14103−14123.
(10) Snir, E.; Joore, J.; Timmerman, P.; Yitzchaik, S. Monitoring Selectivity in Kinase-Promoted Phosphorylation of Densely Packed Peptide Monolayers Using Label-Free Electrochemical Detection. *Langmuir* **2011**, *27*, 11212−11221.
(11) Amit, E.; Obena, R.; Wang, Y.-T.; Zhuravel, R.; Reyes, A. J. F.; Elbaz, S.; Rotem, D.; Porath, D.; Friedler, A.; Chen, Y.-J.; Yitzchaik, S. Integrating Proteomics With Electrochemistry for Identifying Kinase Biomarkers. *Chem. Sci.* **2015**, *6*, 4756−4766.
(12) Chow, E.; Gooding, J. J.; Goading, J. J. Peptide Modified Electrodes as Electrochemical Metal Ion Sensors. *Electroanalysis* **2006**, *18*, 1437−1448.
(13) Tadi, K. K.; Alshanski, I.; Mervinetsky, E.; Marx, G.; Petrou, P.; Dimitrios, K. M.; Gilon, C.; Hurevich, M.; Yitzchaik, S. Oxytocin-Monolayer-Based Impedimetric Biosensor for Zinc and Copper Ions. *ACS Omega* **2017**, *2*, 8770−8778.
(14) Wyttenbach, T.; Liu, D.; Bowers, M. T. Interactions of the Hormone Oxytocin with Divalent Metal Ions. *J. Am. Chem. Soc.* **2008**, *130*, 5993−6000.
(15) Liu, D.; Seuthe, A. B.; Ehrler, O. T.; Zhang, X.; Wyttenbach, T.; Hsu, J. F.; Bowers, M. T. Oxytocin-Receptor Binding: Why Divalent Metals Are Essential. *J. Am. Chem. Soc* **2005**, *127*, 2024−2025.
(16) Pearlmutter, A. F.; Soloff, M. S. Characterization of the Metal Ion Requirement for Oxytocin-Receptor Interaction in Rat Mammary Gland Membranes. *J. Biol. Chem.* **1979**, *254*, 3899−3906.
(17) Bost, M.; Houdart, S.; Oberli, M.; Kalonji, E.; Huneau, J.-F.; Margaritis, I. Dietary Copper and Human Health: Current Evidence and Unresolved Issues. *J. Trace Elem. Med. Biol.* **2016**, *35*, 107−115.
(18) Mocchegiani, E.; Malavolta, M.; Lattanzio, F.; Piacenza, F.; Basso, A.; Abbatecola, A. M.; Russo, A.; Giovannini, S.; Capoluongo, E.; Bustacchini, S.; Guffanti, E. E.; Bernabei, R.; Landi, F. Cu to Zn Ratio, Physical Function, Disability, and Mortality Risk in Older Elderly (IlSIRENTE Study). *AGE* **2012**, *34*, 539−552.
(19) Milanino, R.; Marrella, M.; Gasperini, R.; Pasqualicchio, M.; Velo, G. Copper and Zinc Body Levels in Inflammation: An Overview of the Data Obtained from Animal and Human Studies. *Agents Actions* **1993**, *39*, 195−209.
(20) Malavolta, M.; Giacconi, R.; Piacenza, F.; Santarelli, L.; Cipriano, C.; Costarelli, L.; Tesei, S.; Pierpaoli, S.; Basso, A.; Galeazzi, R.; Lattanzio, F.; Mocchegiani, E. Plasma Copper/Zinc Ratio: An Inflammatory/Nutritional Biomarker as Predictor of All-Cause Mortality in Elderly Population. *Biogerontology* **2010**, *11*, 309−319.
(21) Leone, N.; Courbon, D.; Ducimetiere, P.; Zureik, M. Zinc, Copper, and Magnesium and Risks for All-Cause, Cancer, and Cardiovascular Mortality. *Epidemiology* **2006**, *17*, 308−314.
(22) Díez, M.; Cerdà, F. J.; Arroyo, M.; Balibrea, J. L. Use of the Copper/Zinc Ratio in the Diagnosis of Lung Cancer. *Cancer* **1989**, *63*, 726−730.
(23) Malavolta, M.; Piacenza, F.; Basso, A.; Giacconi, R.; Costarelli, L.; Mocchegiani, E. Serum Copper to Zinc Ratio: Relationship with Aging and Health Status. *Mech. Ageing Dev.* **2015**, *151*, 93−100.
(24) Tadi, K. K.; Alshanski, I.; Hurevich, M.; Yitzchaik, S. Impedimetric Sensing of Copper (II) Ion Using Oxytocin as Recognition Element. *Surfaces* **2018**, *1*, 90−95.
(25) Wink, T.; van Zuilen, S. J.; Bult, A.; van Bennekom, W. P. Self-Assembled Monolayers for Biosensors. *Analyst* **1997**, *122*, 43R−50R.
(26) Widrig, C. A.; Chung, C.; Porter, M. D. The Electrochemical Desorption of N-Alkanethiol Monolayers from Polycrystalline Au and Ag Electrodes. *J. Electroanal. Chem. Interfacial Electrochem.* **1991**, *310*, 335−359.
(27) Grönbeck, H.; Curioni, A.; Andreoni, W. Thiols and Disulfides on the Au(111) Surface: The Headgroup-Gold Interaction. *J. Am. Chem. Soc.* **2000**, 3839−3842.
(28) Lavrich, D. J.; Wetterer, S. M.; Bernasek, S. L.; Scoles, G. Physisorption and Chemisorption of Alkanethiols and Alkyl Sulfides on Au(111). *J. Phys. Chem. B* **1998**, *102*, 3456−3465.
(29) Walczak, M. M.; Popenoe, D. D.; Deinhammer, R. S.; Lamp, B. D.; Chung, C.; Porter, M. D. Reductive Desorption of Alkanethiolate Monolayers at Gold: A Measure of Surface Coverage. *Langmuir* **1991**, *7*, 2687−2693.
(30) Nishizawa, M.; Sunagawa, T.; Yoneyama, H. Selective Desorption of 3-Mercaptopropionic Acid from a Mixed Monolayer with Hexadecanethiol Assembled on a Gold Electrode. *J. Electroanal. Chem.* **1997**, *436*, 213−218.
(31) Heinz, H.; Vaia, R. A.; Farmer, B. L.; Naik, R. R. Accurate Simulation of Surfaces and Interfaces of Face-Centered Cubic Metals Using 12−6 and 9−6 Lennard-Jones Potentials. *J. Phys. Chem. C* **2008**, *112*, 17281−17290.
(32) Malde, A. K.; Zuo, L.; Breeze, M.; Stroet, M.; Poger, D.; Nair, P. C.; Oostenbrink, C.; Mark, A. E. An Automated Force Field Topology Builder (ATB) and Repository: Version 1.0. *J. Chem. Theory Comput.* **2011**, *7*, 4026−4037.
(33) Singh, U. C.; Kollman, P. A. An Approach to Computing Electrostatic Charges for Molecules. *J. Comput. Chem.* **1984**, *5*, 129−145.
(34) Nosé, S. A Unified Formulation of the Constant Temperature Molecular Dynamics Methods. *J. Chem. Phys.* **1984**, *81*, 511−519.
(35) Squire, D. R.; Holt, A. C.; Hoover, W. G. Isothermal Elastic Constants for Argon. Theory and Monte Carlo Calculations. *Physica* **1969**, *42*, 388−397.
(36) VandeVondele, J.; Hutter, J. Gaussian Basis Sets for Accurate Calculations on Molecular Systems in Gas and Condensed Phases. *J. Chem. Phys.* **2007**, *127*, No. 114105.
(37) Krack, M.; Parrinello, M. All-Electron Ab-Initio Molecular Dynamics. *Phys. Chem. Chem. Phys.* **2000**, *2*, 2105−2112.
(38) Hutter, J.; Iannuzzi, M.; Schiffmann, F.; VandeVondele, J. Cp2k: Atomistic Simulations of Condensed Matter Systems. *Wiley Interdiscip. Rev.: Comput. Mol. Sci.* **2014**, *4*, 15−25.
(39) Goedecker, S.; Teter, M.; Hutter, J. Separable Dual-Space Gaussian Pseudopotentials. *Phys. Rev. B* **1996**, *54*, 1703−1710.
(40) Perdew, J. P.; Burke, K.; Ernzerhof, M. Generalized Gradient Approximation Made Simple. *Phys. Rev. Lett.* **1996**, *77*, 3865−3868.
(41) HomelQuantumWise. https://quantumwise.com/ (accessed Sep 16, 2018).
(42) Soler, J. M.; Artacho, E.; Gale, J. D.; Garcia, A.; Junquera, J.; Ordejon, P.; Sanchez-Portal, D. The SIESTA Method for Ab Initio Order-N Materials Simulation. *J. Phys. Condens. Matter* **2002**, *14*, 2745−2779.
(43) Brandbyge, M.; Mozos, J.-L.; Ordejón, P.; Taylor, J.; Stokbro, K. Density-Functional Method for Nonequilibrium Electron Transport. *Phys. Rev. B* **2002**, *65*, No. 165401.
(44) Henkelman, G.; Uberuaga, B. P.; Jónsson, H. A Climbing Image Nudged Elastic Band Method for Finding Saddle Points and Minimum Energy Paths. *J. Chem. Phys.* **2000**, *113*, 9901.

DOI: 10.1021/acs.langmuir.9b01830
Langmuir 2019, 35, 11114−11122

(45) Schlipf, M.; Gygi, F. Optimization Algorithm for the Generation of ONCV Pseudopotentials. *Comput. Phys. Commun.* **2015**, *196*, 36−44.
(46) Kavelin, V.; Fesenko, O.; Dubyna, H.; Vidal, C.; Klar, T. A.; Hrelescu, C.; Dolgov, L. Raman and Luminescent Spectra of Sulfonated Zn Phthalocyanine Enhanced by Gold Nanoparticles. *Nanoscale Res. Lett.* **2017**, *12*, 197.
(47) Bürgi, T. Nanoscale Properties of the Gold-Sulphur Interface: From Self-Assembled Monolayers to Clusters. *Nanoscale* **2015**, *7*, 15553.
(48) Young, A. G.; Green, D. P.; Mcquillan, A. J. IR Spectroscopic Studies of Adsorption of Dithiol-Containing Ligands on CdS Nanocrystal Films in Aqueous Solutions. *Langmuir* **2007**, *23*, 12923−12931.
(49) Torreggiani, A.; Tinti, A. Raman Spectroscopy a Promising Technique for Investigations of Metallothioneins. *Metallomics* **2010**, *2*, 246.
(50) Domènech, J.; Tinti, A.; Capdevila, M.; Atrian, S.; Torreggiani, A. Structural Study of the Zinc and Cadmium Complexes of a Type 2 Plant (Quercus Suber) Metallothionein: Insights by Vibrational Spectroscopy. *Biopolymers* **2007**, *86*, 240−248.
(51) Kedzia, B. B.; Armendarez, P. X.; Nakamoto, K. Infra-Red Spectra and Normal Co-Ordinate Analyses of Metal Biuret Complexes. *J. Inorg. Nucl. Chem.* **1968**, *30*, 849−860.
(52) Huber, H.; Kundig, E. P.; Ozin, G. A. Synthesis and Infrared Spectroscopic Detection of Rhenium Pentacarbonyl. *J. Am. Chem. Soc.* **1974**, *96*, 5585−5586.
(53) Stevens, J. S.; de Luca, A. C.; Pelendritis, M.; Terenghi, G.; Downes, S.; Schroeder, S. L. M. Quantitative Analysis of Complex Amino Acids and RGD Peptides by X-Ray Photoelectron Spectroscopy (XPS). *Surf. Interface Anal.* **2013**, *45*, 1238−1246.
(54) Vericat, C.; Vela, M. E.; Benitez, G.; Carro, P.; Salvarezza, R. C. Self-Assembled Monolayers of Thiols and Dithiols on Gold: New Challenges for a Well-Known System. *Chem. Soc. Rev.* **2010**, *39*, 1805.
(55) Love, J. C.; Estroff, L. A.; Kriebel, J. K.; Nuzzo, R. G.; Whitesides, G. M. Self-Assembled Monolayers of Thiolates on Metals as a Form of Nanotechnology. *Chem. Rev.* **2005**, *105*, 1103−1170.
(56) Sirtori, V.; Zambon, F.; Lombardi, L. XPS and Ellipsometric Characterization of Zinc-BTA Complex. *J. Electron. Mater.* **2000**, *29*, 463−467.
(57) Martin-Vosshage, D.; Chowdari, B. V. R. XPS Studies on (PEO)nLiClO4 and (PEO)nCu(ClO4)2 Polymer Electrolytes. *J. Electrochem. Soc* **1995**, *142*, 1442−1446.
(58) Baltrusaitis, J.; Jayaweera Ac, P. M.; Grassian, V. H. XPS Study of Nitrogen Dioxide Adsorption on Metal Oxide Particle Surfaces under Different Environmental Conditionsw. *Phys. Chem. Chem. Phys.* **2009**, *11*, 8295−8305.
(59) Ukpong, E. J.; Udoetok, I. A.; Nyeneime, W. A. Cyclic Voltammetry of Aqueous Copper (II)- Pentamethyldiethylenetriamine Systems at Various PH Values. *IOSR J. Appl. Chem.* **2013**, *5*, 50−55.
(60) Ozensoy, E.; Meier, D. C.; Goodman, D. W. Polarization Modulation Infrared Reflection Absorption Spectroscopy at Elevated Pressures: CO Adsorption on Pd(111) at Atmospheric Pressures. *J. Phys. Chem. B* **2002**, *106*, 9367−9371.
(61) Gliboff, M.; Sang, L.; Knesting, K. M.; Schalnat, M. C.; Mudalige, A.; Ratcliff, E. L.; Li, H.; Sigdel, A. K.; Giordano, A. J.; Berry, J. J.; Nordlund, D.; Seidler, G. T.; Brédas, J.-L.; Marder, S. R.; Pemberton, J. E.; Ginger, D. S. Orientation of Phenylphosphonic Acid Self-Assembled Monolayers on a Transparent Conductive Oxide: A Combined NEXAFS, PM-IRRAS, and DFT Study. *Langmuir* **2013**, *29*, 2166−2174.
(62) Kong, J.; Yu, S. Fourier Transform Infrared Spectroscopic Analysis of Protein Secondary Structures. *Acta Biochim. Biophys. Sin.* **2007**, *39*, 549−559.
(63) Barth, A. Infrared Spectroscopy of Proteins. *Biochim. Biophys. Acta, Bioenerg.* **2007**, *1767*, 1073−1101.
(64) Häkkinen, H. The Gold−Sulfur Interface at the Nanoscale. *Nat. Chem.* **2012**, *4*, 443−455.
(65) Zenou, N.; Zelichenok, A.; Yitzchaik, S.; Cohen, R.; Cahen, D. Tuning the Electronic Properties of Silicon via Molecular Self-Assembly. *ACS Symp. Ser.* **1998**, 57−66.
(66) He, T.; Ding, H.; Peor, N.; Lu, M.; Corley, D. A.; Chen, B.; Ofir, Y.; Gao, Y.; Shlomo Yitzchaik, A.; Tour, J. M. Silicon/Molecule Interfacial Electronic Modifications. *J. Am. Chem. Soc* **2008**, *130*, 1699−1710.
(67) Peor, N.; Sfez, R.; Yitzchaik, S. Variable Density Effect of Self-Assembled Polarizable Monolayers on the Electronic Properties of Silicon. *J. Am. Chem. Soc.* **2008**, *130*, 4158−4165.
(68) Sfez, R.; Peor, N.; Yitzchaik, S. Experimental Evidence of Molecular Cooperative Effect in a Mixed Parallel and Antiparallel Dipole Monolayer. *J. Phys. Chem. C* **2010**, *114*, 20531−20538.
(69) Gankin, A.; Sfez, R.; Mervinetsky, E.; Buchwald, J.; Dianat, A.; Medrano Sandonas, L.; Gutierrez, R.; Cuniberti, G.; Yitzchaik, S. Molecular and Ionic Dipole Effects on the Electronic Properties of Si-/SiO2 -Grafted Alkylamine Monolayers. *ACS Appl. Mater. Interfaces* **2017**, *9*, 44873−44879.
(70) Gankin, A.; Mervinetsky, E.; Alshanski, I.; Buchwald, J.; Dianat, A.; Gutierrez, R.; Cuniberti, G.; Sfez, R.; Yitzchaik, S. ITO Work Function Tunability by Polarizable Chromophore Monolayers. *Langmuir* **2019**, *35*, 2997−3004.
(71) Kim, H. K.; Hyla, A. S.; Winget, P.; Li, H.; Wyss, C. M.; Jordan, A. J.; Larrain, F. A.; Sadighi, J. P.; Fuentes-Hernandez, C.; Kippelen, B.; Brédas, J. L.; Barlow, S.; Marder, S. R. Reduction of the Work Function of Gold by N-Heterocyclic Carbenes. *Chem. Mater.* **2017**, *29*, 3403−3411.
(72) Natan, A.; Kronik, L.; Shapira, Y. Computing Surface Dipoles and Potentials of Self-Assembled Monolayers from First Principles. *Appl. Surf. Sci.* **2006**, *252*, 7608−7613.
(73) Deutsch, D.; Natan, A.; Shapira, Y.; Kronik, L. Electrostatic Properties of Adsorbed Polar Molecules: Opposite Behavior of a Single Molecule and a Molecular Monolayer. *J. Am. Chem. Soc.* **2007**, *129*, 2989−2997.
(74) Oren, R.; Sfez, R.; Korbakov, N.; Shabtai, K.; Cohen, A.; et al. Electrically Conductive 2D-PAN-Containing Surfaces As. *J. Biomater. Sci., Polym. Ed.* **2004**, *15*, 1355−1374.

DOI: 10.1021/acs.langmuir.9b01830
Langmuir 2019, 35, 11114−11122